On the viscous resistance of ships sailing in shallow water

Zeng, Qingsong; Hekkenberg, Robert; Thill, Cornel

DOI
10.1016/j.oceaneng.2019.106434

Publication date
2019

Document Version
Accepted author manuscript

Published in
Ocean Engineering

Citation (APA)
Zeng, Q., Hekkenberg, R., & Thill, C. (2019). On the viscous resistance of ships sailing in shallow water. *Ocean Engineering*, *190*, Article 106434. https://doi.org/10.1016/j.oceaneng.2019.106434

On the viscous resistance of ships sailing in shallow water

Qingsong Zeng*, Robert Hekkenberg, Cornel Thill
Delft University of Technology, 2628CD, Delft, the Netherlands

Abstract

Accurate resistance prediction for ships sailing in vertically restricted waterways is highly required to improve the design and operation for large ships entering harbors and for vessels navigating in inland waters. The methods derived from deep water may lead to large errors, and studies considering shallow water effects are needed. As most ships sailing in shallow water operate at a low Froude number, the viscous resistance dominates the total resistance and becomes the main concern. In this study, a Wigley hull and the KCS (KRISO Container Ship), which have available benchmark data, are applied. A typical 86m long inland ship is then chosen to further investigate the influence of a different hull form. Results show that the friction and the viscous pressure resistance depend on ship types, speeds, and water depths. A formula to predict a ship's friction in shallow water is given with some constants determined based on ship's characteristics. A form factor defined based on computed ship's friction is suggested, and an empirical expression is provided for each ship applied. With the investigations for three ship forms, this study is expected to provide inspirations to further improve the prediction of ship's viscous resistance in shallow water.

Keywords: Shallow water; viscous resistance; form factor; inland ship; CFD

List of symbols

$1+k$ = Form factor

$1+k^*$ = Modified form factor

B = Beam of a ship (m)

B_C = Blockage coefficient

C_B = Block coefficient

C_f = Coefficient of frictional resistance

C_{f_c} = Computed friction coefficient

C_v = Coefficient of the viscous resistance

CFD = Computational Fluid dynamics

h = Water depth (m)

I = Turbulence intensity

L = Length of a flat plate (m)

L_{pp} = Perpendicular length of a ship (m)

p = Order of accuracy

Re = Reynolds number

S = Wetted surface (m^2)

S_{RE} = Standard deviation

T = Draft of a model or a ship (m)

u^* = Shear velocity (m/s)

$U(\phi_i)$ = Uncertainty of a variable ϕ_i

V = Velocity of the incoming water (m/s)

y^+ = y plus, a non-dimensional wall distance

α = A parameter which identifies the grid cell size

μ = Molecular dynamic viscosity (Pa·s)

μ_t = Turbulent viscosity (Pa·s)

v= Kinematic viscosity (m^2/s)

1 Introduction

Predicting the resistance accurately is essential for ship design and operation. For inland vessels and for large ships sailing in coastal waters and ports, it is known that the limited water depth will influence ship resistance in different extent (Jiang, 2001; Lackenby, 1963; Schlichting, 1934). Prediction methods derived from deep water, e.g., the approach of Holtrop and Mennen (1982), become less applicable since the effects of shallow water are not considered.

* Corresponding author.
E-mail address: Q.Zeng@tudelft.nl (Q.Zeng).

During ship model tests, the conventional way to deal with ship resistance is based on Froude's approach, where the resistance is divided into two independent parts, the viscous resistance component and the wave resistance component (ITTC, 2011). The viscous part is assumed to be proportional to the frictional resistance: $(1+k)C_f$, where the C_f is the frictional resistance coefficient, which is usually calculated by the ITTC 57 correlation line (ITTC, 1957) and $1+k$ is the form factor. In the model-ship extrapolation, the $1+k$ is conventionally assumed to be independent on Reynolds number (Re) .

The ITTC57 correlation line is, strictly speaking, not a friction line for flat plates. It contains some form effects and has a larger value at model scale if compared with normal friction lines, for instance, the formula proposed by Grigson (1999) and Katsui et al. (2005). However, all of these lines were designed for deep water. When a ship sails in shallow water, the friction on ship hull is altered due to shallow water effects. In the research of Zeng et al. (2019), restrict water conditions are built for a 2D flat plate by imposing a parallel wall close the plate. It was shown that, for the same Re, the C_f can increase by 50% for the lowest Re and 10% for the highest Re when the two walls are close enough to each other. It means the C_f also depends on the size of space where the fluid passes. The restrict water condition acts as another form effects on the C_f, and its effects on friction can also to be included in the correlation line. As the research of Zeng et al., C_f was derived from a 2D flat plate, its accuracy is somewhat affected by the absence of 3D flow effects. The current study extended such research to 3D condition. The effects of water depth on a 3D ship hull and how the ship form plays a role on C_f have been analyzed by considering three ship types in various water depths.

For the $1+k$, the ideal condition is that it stays the same for both full scale and model scale, but actually, it depends on Re (García-Gómez, 2000) and also depends on the chosen correlation line (Van der Ploeg et al., 2008). As indicated by ITTC (2008), the form factor is less dependent on Re when the Grigson (1999) line is used instead of ITTC57 line, but this is not enough to determine which one is better than another. In shallow water, it was found that the $1+k$ also depends on water depth. Based on model tests, Millward (1989) suggested an empirical correction for $1+k$ in different water depths. The CFD simulations performed by Toxopeus (2011) supported Millward's formula and indicate that the $1+k$ of the KVLCC2 can increase by about 30% in shallow water. Raven (2012) showed that the treatment of the form factor is crucial for the accuracy of the extrapolation of ship resistance from model to full scale, and an empirical correction is also proposed (Raven, 2016). However, a systematic study of $1+k$ in the whole Re range of ships considering shallow water effects is rare, which will be addressed in this study.

Additionally, immersed transom is another important factor that affects the form factor (Hollenbach, 2009). The transom, as well as tunnel endings, are commonly found for inland ships and their effects on ship resistance are difficult to separate from the total resistance. In this paper, a ship with a transom is added and the effects of the transom are incorporate into a newly-defined form factor. Based on this study, practically useful conclusions can be determined for those ships with an immersed transom.

In this study, double-body calculations are performed using Computational Fluid Dynamics (CFD). By suppressing the free surface, the method allows the study of form effects even at higher speeds. Seven shallow water conditions are generated by adjusting the position of the water bottom. A deep-water case is added for comparison. Twelve Reynolds numbers in the range of 10^5 to 10^9 are used, which can cover both model scale to full scale. After comparing with the viscous resistance on a 2D flat plate, the effects of the curved surface of a ship are discussed. The comparisons of the viscous resistance of a Wigley hull, the KCS (KRISO Container Ship) and an inland ship in various water depths provide insight into form effects on both the C_f and $1+k$. Empirical formulas are fitted to build an improved prediction of resistance of the three chosen ships.

This paper consists of five parts. Part 2 presents the method that is used as well as the parameters of the models applied. Part 3 provides the verification and validation of the numerical simulations. Part 4 analyzes the results of the CFD simulations and develops empirical formulas for different components of the viscous resistance. Conclusions are drawn in Part 5.

2 Method

The presence of the bare bottom of the fairway, which can alter the frictional resistance in a way that been cursorily analyzed, might be understood as a kind of form effect. As this effect is even traceable at flat plates free of any curvature, this effect is here considered by a modified friction line. Furthermore, the viscous pressure resistance is affected by the presence of the bottom as well; this effect will

here be considered in terms of a modified form factor $1+k^*$. In the following, studying the effects of water depth is the purpose and a strategy is introduced in the first subsection. Afterward, the details of the geometric models used in this investigation are introduced.

2.1 The strategy of comparison

Although the empirical friction lines exist, a numerical friction line derived from the simulations on a 2D flat plate is applied for further analysis, to avoid the effects of modeling errors between empirical friction lines and numerical calculations.

As for ship types, a mathematical "standard" ship, the Wigley hull, is used due to a large amount of benchmark data. In addition to that, since the Wigley hull is too slender to represent most inland ships, a typical inland ship was added: the Rhine ship 86, which will be introduced in detail later. Since the block coefficient (C_B) of these two ships are 0.45 and 0.86, respectively, which represent the two extremes, a ship with an intermediate value is selected: the KCS (KRISO Container Ship), where C_B = 0.65. The difference between different ship forms can help to reveal the influence of the ship type or, specifically, the area of the flat bottom on the viscous resistance in shallow water. The strategy of this study is outlined in **Fig. 1**.

The Reynolds number (*Re*) is one of the control dimensionless variables in this study. Generally, the magnitude of *Re* of a ship model is at the level of 10^6 and for a full-scale ship, the number is 10^8. Since the results of resistance of ship models are more sensitive to *Re*, more sampling points will be given for relatively low Reynolds number, which is shown in **Table 1**.

Table 1 The chosen Reynolds number (*Re*) in this study

No.	lg(*Re*)	*Re*
1	5.8	6.310×10^5
2	6.0	1.000×10^6
3	6.2	1.585×10^6
4	6.4	2.512×10^6
5	6.6	3.981×10^6
6	6.8	6.310×10^6
7	7.2	1.585×10^7
8	7.6	3.981×10^7
9	8.0	1.000×10^8
10	8.4	2.512×10^8
11	8.8	6.310×10^8
12	9.2	1.585×10^9

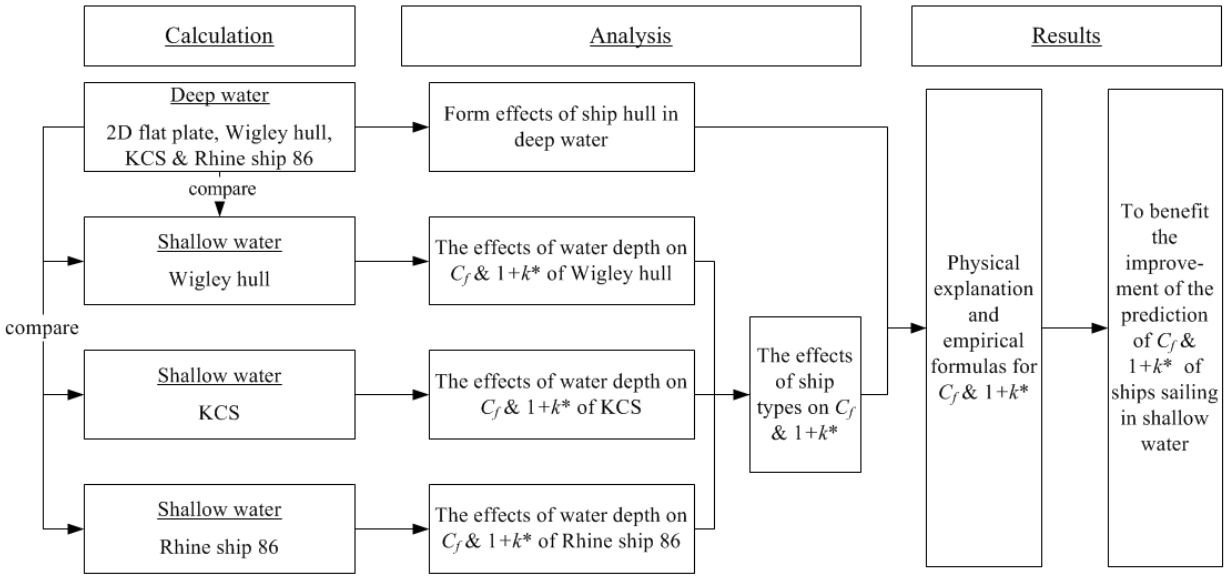

Fig. 1 The strategy of comparison in this study (C_f: the coefficient of the frictional resistance; $1+k^*$: the modified form factor)

2.2 The models

In this section, the models of a 2D flat plate, a Wigley hull, the KCS, and an inland ship are introduced.

2.2.1 The 2D flat plate

The computational model of the 2D flat plate and the boundary conditions are shown in **Fig. 2**.

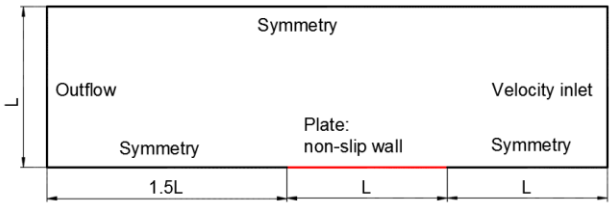

Fig. 2 The computational domain of for the 2D flat plate and the boundary conditions

The computational domain extends one plate length (L) in front of the plate, 1.5L in the rear and L at the side. As indicated in Zeng et al. (2019), such size of the domain is large enough for C_f calculations, and the shallow water effects are negligible.

2.2.2 The Wigley hull, the KCS and the Rhine Ship 86

The hull surface of a Wigley hull can be described mathematically as

$$y = \frac{B}{L}\left(1-\left(\frac{2x}{L}\right)^2\right)\left(1-\left(\frac{z}{T}\right)^2\right), \quad (1)$$

where B is the beam, L the length, and x, y, z are the coordinates of three directions. The x is positive forward, y is positive port and z is positive upward. The origin is at the cross point of the aft perpendicular and the zero-waterline plane. This coordinate system also applies for the KCS and the Rhine Ship 86.

Table 2 The main dimensions of the Wigley ship, the KCS, and the Rhine Ship 86

	Unit	Wigley ship	KCS	Rhine Ship 86
L_{pp}	m	2.500	230.000	85.522
B	m	0.250	32.200	11.400
T	m	0.156	10.800	3.500
C_B	-	0.445	0.651	0.860
S	m^2	0.930	9530.000	1418.761

(L_{pp}: Length between the perpendiculars; B: Beam; C_B: block coefficient; S: Area of the wetted surface)

The sketches of sections of the Wigley hull (Ship A), the KCS (Ship B), and the Rhine Ship 86 (Ship C) are shown in **Fig. 3**. Because the total length of the ship is 86m, we named it as "Rhine Ship 86". The main dimensions of the chosen ships are listed in **Table 2**.

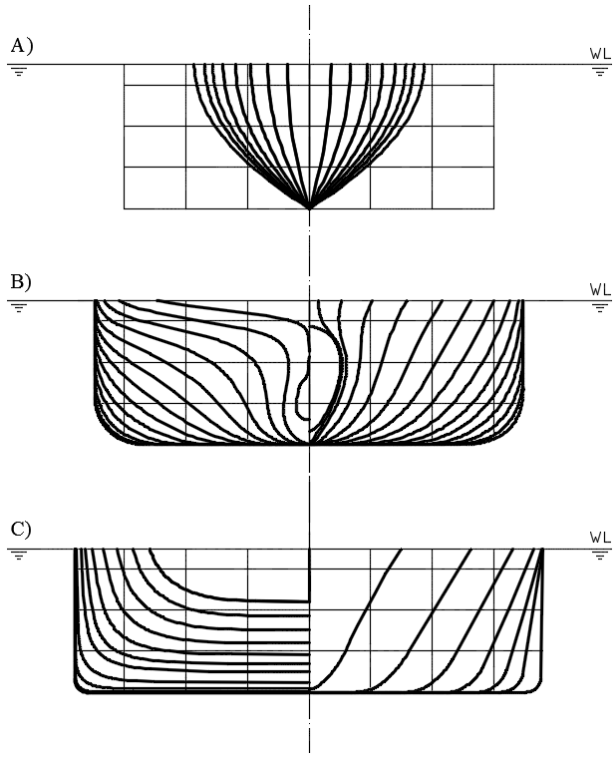

Fig. 3 The sections of A) the Wigley hull, B) the KCS, and C) the Rhine Ship 86

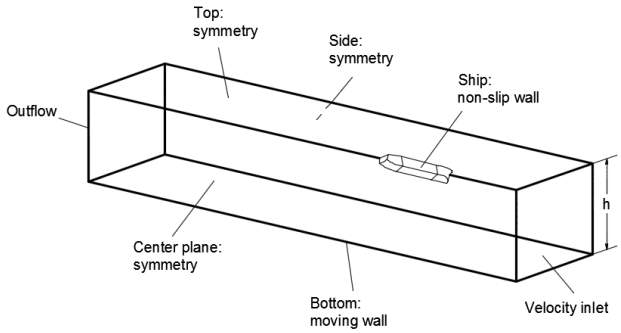

Fig. 4 The computational model and boundary conditions for the ships (h: water depth)

The computational domain, which is shown in **Fig. 4**, extends 3 L_{pp} in the rear. It will not affect the computation of C_f on the ship and also can satisfy the outlet boundary layer. The side boundary should be set far enough to avoid blockage effects. To search for an appropriate position, calculations were performed for KCS with the side

boundary deviate by $0.5L_{pp}$, $1.0L_{pp}$, $1.5L_{pp}$, $2.0L_{pp}$, and $3.0L_{pp}$ from the ship. In addition, one ship length in front of the ship was found to be sufficient to prevent a severe upwind effect of the object to the inlet boundary. Whether a position further than $1.0L_{pp}$ will affect the result is also studied by setting the inlet boundary at $1.5L_{pp}$, $2.0L_{pp}$, and $3.0L_{pp}$ in front of the object. At the inlet boundary for Cases 1 through 8, the initial turbulent intensity is 6% and the turbulent viscosity ratio (μ/μ_t) is 100, which follows the suggestion of Zeng et al. (2019). For Case 9, the initial turbulent intensity is 2.6% and the turbulent length scale is 3 L_{pp}, by which the level of the turbulent intensity in front of the ship is similar to Case 5. The results of C_f for all cases are compared in **Table 3**.

Table 3 Results of C_f of the KCS with different locations of the side and front boundary (h/T = 1.2, lgRe = 6.4, y^+ = 2)

Case	Side ($\times L_{pp}$)	Front ($\times L_{pp}$)	B_C* (%)	I** (%)	C_f ($\times 10^{-3}$)	Error Vs. Case 5
1	0.5	1.0	11.67	0.84	4.502	6.35%
2	1.0	1.0	5.83	0.84	4.265	0.76%
3	1.5	1.0	3.89	0.84	4.236	0.08%
4	2.0	1.0	2.92	0.84	4.233	-0.01%
5	3.0	1.0	1.94	0.84	4.233	0.00%
6	3.0	1.5	1.94	0.60	4.171	-1.46%
7	3.0	2.0	1.94	0.49	4.140	-2.19%
8	3.0	3.0	1.94	0.38	4.117	-2.75%
9***	3.0	3.0	1.94	0.85	4.232	-0.03%

(*B_C: blockage coefficient, the ratio between the area of the ship midsection and the area of the waterway section;
**I: The turbulent intensity recorded at 0.5 L_{pp} in front of the ship with y = 0 at the compressed water surface;
***Case 9: An additional case based on Case 8 by increasing the I to a similar level to Case 5.)

Some remarks can be derived based on **Table 3**. For the position of the side boundary (Cases 1 through 5):

- When it locates at $0.5L_{pp}$, the B_C is 11.7% and the error of C_f is significant (6.35%);
- When the side boundary is $1.0L_{pp}$ away from the ship, its influence on C_f is negligible (less than 1%);
- Changing the location of the side boundary in the range of 0.5 L_{pp} ~ 3.0 L_{pp} has no influent on the turbulent intensity in front of the vessel;
- If a stricter accuracy of C_f is needed (e.g., less than 0.1%), the B_C should be less than 3.9%;
- If the Blockage is less 3.9%, further reducing the B_C makes little contribution to the C_f.

In this study, the B_C is guaranteed to be equal to or less than 3.9%. For the KCS at $1.2 \leq h/T \leq 2.0$, the side boundary is set at 1.5 L_{pp} away from the ship's centerline. For the Rhine Ship 86, a value of 1.5 L_{pp} applies for $1.2 \leq h/T \leq 1.5$. For other cases, the side boundary is at 1.0 L_{pp}.

For the position of the front boundary (Cases 2 to 9):

- When the B_C is less than 5.8%, the result of C_f is more sensitive to the position of front boundary than that of the side boundary;
- The further away the front boundary, the lower the C_f. This can be explained by the level of turbulence intensity (I) of the upcoming flow, of which the values are 0.84%, 0.60%, 0.49%, and 0.38% for $1.0L_{pp}$, $1.5L_{pp}$, $2.0L_{pp}$, and $3.0L_{pp}$;
- In Case 9, the I of the upcoming flow is increased to 0.85% and the rest settings are the same as Case 8. It can be found that the C_f of Case 9 has a minor difference from Case 5, which means the turbulent intensity, instead of the position of the front boundary, dominates the changes of C_f. Therefore, Case 5 is preferred due to fewer grid cells and thus less computing time.

In the simulations of this study, the flow enters the inlet boundary was set to be unidirectional and the turbulence intensity, therefore, decays fast before reaching the ship. For a natural river or canal, the level of turbulence intensity close to the water surface is usually more than 1% (Kozioł, 2013). To make sure the turbulence intensity is as close as the natural condition, the front boundary at $1.0L_{pp}$ is preferred and used for all simulations in this study. Since a distance less than $1.0L_{pp}$ is less likely to cope with the backflow, such condition is not considered.

By adjusting the value of h, seven water depths are selected and shown in **Table 4**.

Table 4 The seven water depths selected in this study

No.	h/T
1	15.06
2	4.00
3	3.00
4	2.00
5	1.80
6	1.50
7	1.20

(h: Water depth; T: Draft of the ship)

2.3 Mesh generation and the solver

The structured mesh type is applied to all computations in this study. Grids close to a non-slip wall are refined to capture the flow variables with larger gradients, and an example is shown in **Fig. 5**. For shallow water cases, the number of grid points in the vertical direction is adjusted according to the water depths. For high Reynolds number cases, the mesh is refined in the *x* direction correspondingly to keep the aspect ratio of the mesh cells at an acceptable level.

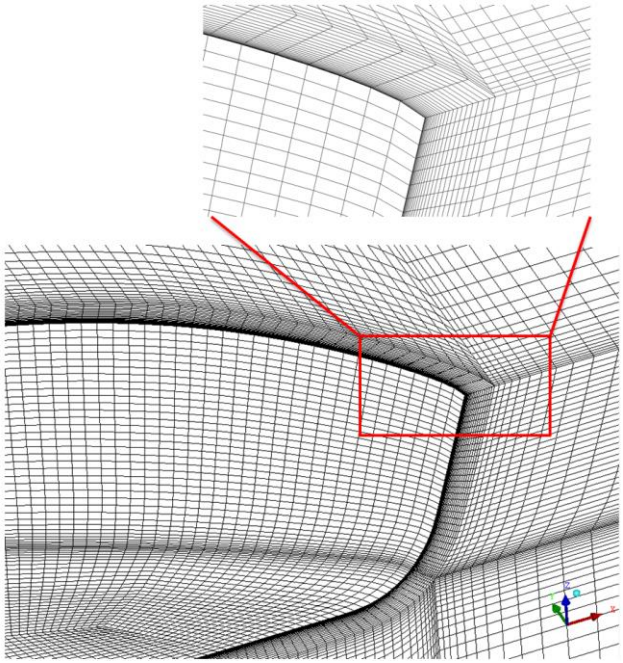

Fig. 5 The mesh around the bow of the Rhine Ship 86

In this study, all numerical calculations were performed in an FVM (Finite Volume Method) code ANSYS Fluent (version 18.1). The SST k-ω model is chosen as the turbulence model. The scheme of the pressure-velocity coupling is "Coupled" and the discretization of the gradient is "Least Squares Cell-Based". "PRESTO!" is used for the discretization of pressure, and "Second Order Upwind" is applied for the discretization of momentum, turbulent kinetic energy, and specific dissipation rate.

3 Verification and validation

In this section, a grid independence study is performed to verify the mesh and the RANS solver. Afterward, the calculations of the frictional resistance of ships are validated with the existing empirical formulas.

3.1 Verification

The calculation should be verified to keep the numerical errors at an acceptable level. When double precision format and suitable convergence criteria are used, the dominant error is the discretization error (Eça and Hoekstra, 2009) and becomes the main target in this subsection.

According to Roache (1998), a grid refinement study is an effective way to find the most suitable mesh for calculations. In this verification, four geometrically similar grids (G1 to G4) were built for the 2D flat plate as well as the three ship hulls. The refinement ratio for each direction is 1.25 and the finest grid is G1. A factor α is defined by multiplying the refinement ratio at different times. It can be used to indicate the density of the mesh (the smaller the finer). **Table 5** shows the number of nodes in the *x*, *y* and *z* directions for all cases.

Table 5 Number of nodes in *x*, *y* and *z* directions for the 2D flat plate, the Wigley hull, the KCS, and the Rhine ship 86 (deep water)

	No.	*x*	*y*	*z*	*α*	Total cells (million)
2D flat plate	G1	881	250	-	1.00	0.22
	G2	701	198	-	1.25	0.14
	G3	557	158	-	1.56	0.09
	G4	449	126	-	1.95	0.06
Wigley hull	G1	558	98	122	1.00	6.45
	G2	403	78	98	1.25	3.30
	G3	350	62	78	1.56	1.69
	G4	274	50	66	1.95	0.87
KCS	G1	523	74	168	1.00	8.22
	G2	415	58	132	1.25	4.28
	G3	327	46	96	1.56	2.27
	G4	267	38	84	1.95	1.19
Rhine ship 86	G1	557	65	110	1.00	7.42
	G2	449	53	90	1.25	3.80
	G3	357	41	70	1.56	1.95
	G4	289	33	50	1.95	1.00

The coefficients of the frictional resistance for each grid are compared in **Fig. 6**.

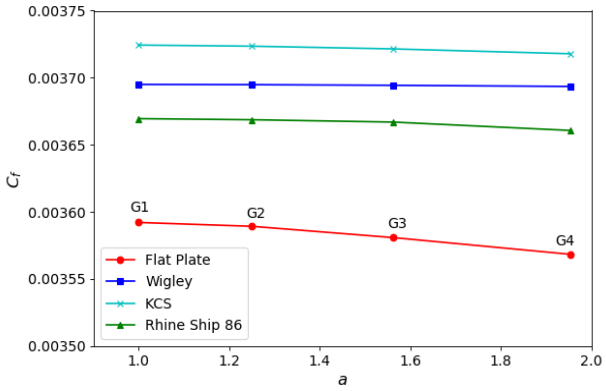

Fig. 6 Frictional resistance coefficient C_f with Grid refinement (deep water, lgRe = 6.4, y^+ = 2)

The curves shown in **Fig. 6** can be fitted by the method of Eça and Hoekstra (2014):

$$S_{RE}(\phi_0, \beta, p) = \sqrt{\sum_{i=1}^{N} (\phi_i - (\phi_0 + \beta \alpha_i^p))^2} \quad , \tag{2}$$

where the ϕ_0, β, p are constants derived from the fitting. The uncertainty is calculated by

$$U(\phi_i) = F_s \left|(\phi_i - \phi_0)\right| + S_{RE} + \left|\phi_i - (\phi_0 + \beta \alpha_i^p)\right|, \tag{3}$$

where the F_s = 1.25 if 0.5 ≤ p < 2.1, otherwise, F_s = 3.

Generally, the accuracy of a calculated frictional resistance increases with the refinement of mesh. However, when it reaches a certain accuracy, continued refinements of the mesh will not obviously contribute to the accuracy but will increase the required computing sources. Therefore, instead of searching for the largest possible number of grid cells, a suitable number with an acceptable error is the purpose of this verification.

After balancing the accuracy and required computing effort of the four types of mesh, the grid G1 is selected for the 2D flat plate, G2 is selected for all chosen ships. The corresponding order of accuracy (p) and the uncertainties ($U(\phi_i)$) are given in **Table 6**.

Table 6 The observed order of accuracy and uncertainty of C_f for the 2D flat plate, the Wigley hull, the KCS, and the Rhine ship 86

	p	$U(\phi_i)$	$U(\phi_i)/\phi_i$
2D flat plate	2.73	1.814×10^{-5}	0.50%
Wigley hull	2.82	8.385×10^{-7}	0.02%
KCS	2.93	5.004×10^{-6}	0.13%
Rhine Ship 86	3.83	4.359×10^{-6}	0.12%

Based on **Table 6**, the orders of accuracy are fine and the uncertainties are at a low level. It means that the chosen girds are acceptable and are deemed sufficient for further simulations.

3.2 Validation

After successfully verifying the simulations, the modeling error should be checked. This error presents the derivation of the numerical results from the experimental data. In this section, calculations are performed with various y^+ and are compared with existing empirical methods to validate the C_f. Afterward, the computations of the form factor with its conventional definition are validated.

3.2.1 Validation of friction

The non-dimensional distance of the first grid cell, which is known as y^+, is defined as follows:

$$y^+ = \frac{u^* y}{\upsilon} \tag{4}$$

where the y is the distance to the wall, u^* the shear velocity and v the kinematic viscosity. The y^+ less than 5 represent the viscous sublayer and 30 ≤ y^+ ≤ 200 indicates the log-law region (Pope, 2000). It is noteworthy that for Finite Volume Method (FVM), y^+ should be calculated at the center of first-layer cells.

For numerical simulations, the y^+ is usually suggested to be as low as 1 to capture more flow details. However, the first layer of cells has a very small height if the Re is high. For example, for the Wigley hull with y^+ = 0.5 and Re = 2.512×10^8, the height of the first-layer cell is 3.289×10^{-7} m, but the length is at the level of 10^{-2} m. The aspect ratio, consequently, is as high as 10^5 which influences the stability and accuracy of numerical simulations. Even an aspect ratio of 10^4 is guaranteed, the number of cells goes to 9 million which leads to an expensive computation. However, if y^+ = 2, the number can reduce to 7 million; if y^+ = 35, the number is 3 million. As the value of y^+ can largely influence the computing efforts, the influence of y^+ on the C_f is studied.

To illustrate whether a higher y^+ can be accepted, the y^+ dependency of C_f is studied. In the calculations, the ω-equation is used in the turbulence model. This enables the wall treatment by blending the viscous sublayer formulation and the logarithmic layer formulation based on y^+ (ANSYS, 2017). In **Fig. 7**, the results of C_f of the 2D plate, the Wigley hull and the KCS calculated in varied y^+ are shown at three Reynolds numbers. Katsui et al. (2005)

and the ITTC57 model-ship correlation line are used for comparison. The values of y^+ vary at sublayer ($y^+ < 5$) and log-law region ($30 \leq y^+ \leq 200$).

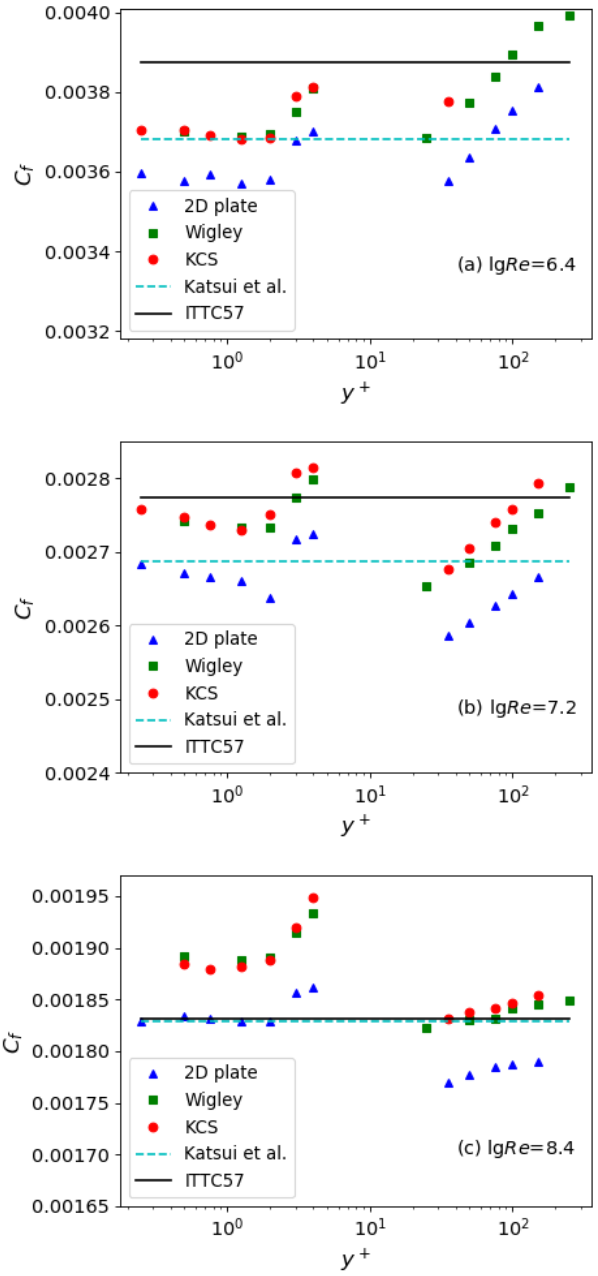

Fig. 7 The results of C_f in varied y^+ for (a): lgRe = 6.4, (b): lgRe = 7.2, and (c): lgRe = 8.4 (deep water)

Some remarks can be derived from **Fig. 7**:

- Minor differences are found for the calculated C_f between the two chosen ships, despite the quite different ship forms;
- For $y^+ < 5$, the results of C_f of both the flat plate and the ships are more stable than those in the log-law region, especially for lgRe = 6.4 and 8.4, where the differences to each other are less than 1%;
- For $30 \leq y^+ \leq 200$, larger differences are observed but the errors (less than 4%) are still practically acceptable;
- From the verification perspective, $y^+ < 1$ should be selected as the benchmark since it directly resolves the boundary layer. Based on this, results generated with the $y^+ < 5$ are more accurate and stable than $30 \leq y^+ \leq 200$;
- From the validation perspective, the numerical results should be compared with the existing experiments. If the friction line proposed by Katsui et al. (2005) is used as the benchmark for both the 2D flat plate and ships, $y^+ < 5$ can give better results than $30 \leq y^+ \leq 200$ at lgRe = 6.4 and 7.2; If the ITTC57 correlation line is used as the benchmark for ships, calculations with $y^+ < 5$ behave better only for lgRe = 7.2.

In summary, the first grid point that locates in the viscous sublayer or the log-law region can both give acceptable results, but the setting of $y^+ < 5$ is preferred due to more stable and physical results. As mentioned above, a relatively higher y^+ can help to reduce the grid cells and consequently save the computing efforts. Therefore, the y^+ = 2 is chosen for all simulations of the flat plate and the ships subsequently.

The water bottom is another non-slip wall and the mesh close to it is also refined. Since it is moving at the same speed as the incoming water, the Reynolds number defined with the relative velocity (to the water) is low and therefore a small y^+ (≈ 1) is easily guaranteed in all cases.

3.2.2 Validation of form factor

The conventional definition of form factor is shown as follows:

$$1+k = \frac{C_v}{C_f}. \tag{5}$$

where the C_v is the coefficient of the viscous resistance, which is the sum of the frictional resistance and the viscous pressure resistance. For the C_f, there was a debate on which line should be used to determine the $1+k$ (ITTC, 2008), but finally a true turbulent flat plate friction line instead of the ITTC57 correlation line was suggested (ITTC, 2017), because the $1+k$ is more dependent on Reynolds number if the ITTC57 line is used.

In this study, the values of 1+k in deep water for the Wigley hull, the KCS, and the Rhine Ship 86 are compared with the experimental data derived from the model tests of Kajitani et al. (1983), Lee et al. (2018), and Zeng et al. (2018), as shown in **Fig. 8**. The experimental form factor (1+k) is calculated with the method of Prohaska (1966) and is assumed to be constant.

In shallow water, two empirical expressions are used to validate the computed form factor. Based on ship model tests, Millward (1989) proposed a modification of form factor considering shallow water effects as follows:

$$\Delta k = 0.644(h/T)^{-1.72} \tag{6}$$

More recently, Raven (2016) fitted a new line for form factor correction in shallow water based on double-body computations for different ship types, both model scale and full scale, as shown in equation (7):

$$(1+k)/(1+k)_{deep} = 1+0.57(h/T)^{-1.79} \tag{7}$$

where the h is water depth and the T is ship draft. The equation (7) was indicated to be valid for $h/T > 2.0$.

Comparisons (**Fig. 8**) are made between the computed form factor in shallow water and the empirical formulas for the Wigley hull, the KCS, and the Rhine Ship 86 at lg(Re)=6.4. The value of C_f on the 2D flat plate is used for calculating 1+k since it uses the same turbulence model and the same y^+ value as used in the ship simulations.

It can be derived from **Fig. 8** that:

- For the Wigley hull, the calculated 1+k in deep water is slightly larger than the experiment (3.2%) but it is practically acceptable. In shallow water, the values of 1+k are smaller than empirical methods. This is due to much fuller ships which were used to derive two empirical methods.
- For the KCS and Rhine Ship 86, the calculated 1+k have a good agreement with experimental and empirical data in both deep and shallow water. It means at least for these two ships, the numerical simulations for 1+k are practically reliable.
- It was indicated that the method of Raven (2016) is only valid for $h/T > 2.0$, but it works well even for $h/T > 1.2$ based on this study.

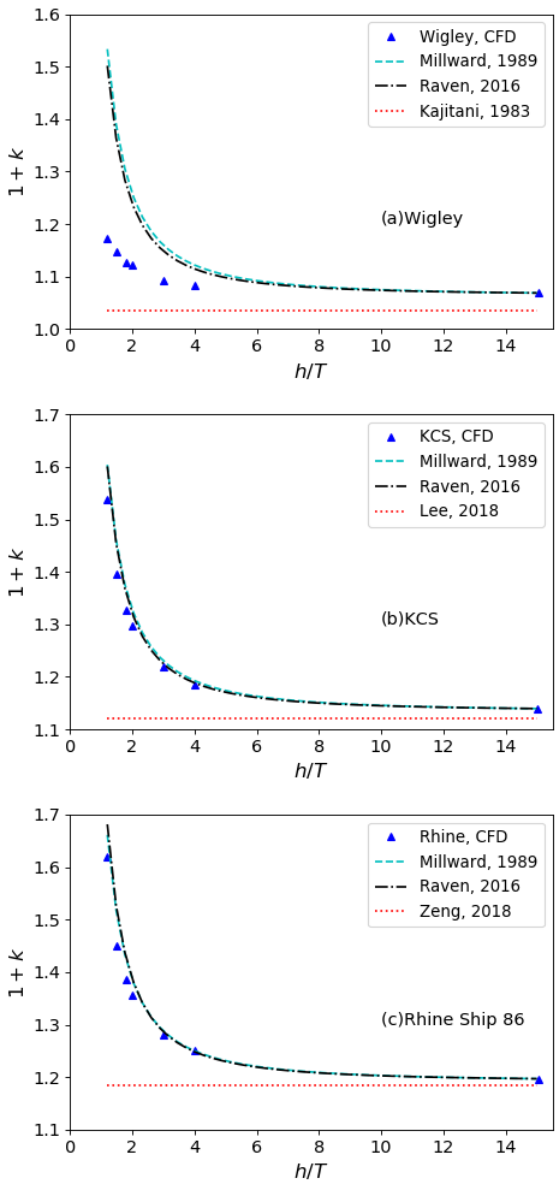

Fig. 8 Comparisons between calculated 1+k and empirical methods for (a): Wigley hull, (b): KCS, and (c): Rhine ship 86 (lg(Re)=6.4, y^+ = 2)

Although shallow water effects on the form factor are corrected in the empirical methods, the Reynolds number dependency (scale effects) are not considered simultaneously. This study moves one step forward to consider the Reynolds number, and details will be addressed in Section 4.2.

4. Results and analysis

In this part, numerical results of the frictional resistance of the 2D flat plate and the ships in deep water are first

compared to demonstrate the form effects of a ship hull. Afterward, shallow water effects on ship's friction are analyzed and the water depth is included in the new correlation line. A different concept of the form factor will be introduced and its value of the three chosen ships are discussed separately.

4.1 The frictional resistance

4.1.1 Comparison between the flat plate and the ships

For the frictional resistance, the crucial difference between a flat plate and a ship is the curved surface. In **Fig. 9**, the results of the frictional resistance coefficient (C_f) against the base-10 logarithm of Reynolds number (lgRe) are shown in deep water.

Some remarks can be made based on **Fig. 9**:

- The form effects are only recognizable at the lower region lgRe < 7.6 of the Re and the effects are decreasing with an increasing Re;
- As one might expect, the values of C_f of the chosen three ships are highly overlapped which means the C_f only depend on the Re in deep water regardless of the ship types.

A friction line derived from a flat plate is usually used to predict the friction of a ship hull with the same length and the same wetted surface (equivalent flat plate assumption). However, based on the results shown in **Fig. 9**, friction derived from a 2D flat plate will underestimate the frictional resistance of a ship, especially at the model scale. This is caused by the effects of the ship's curved surface.

When the ship sails in shallow water, the presence of the water bottom further affects the ship's friction. It plays a similar role to the curved surface and acts as an additional form effect. This will be introduced in detail in the next section.

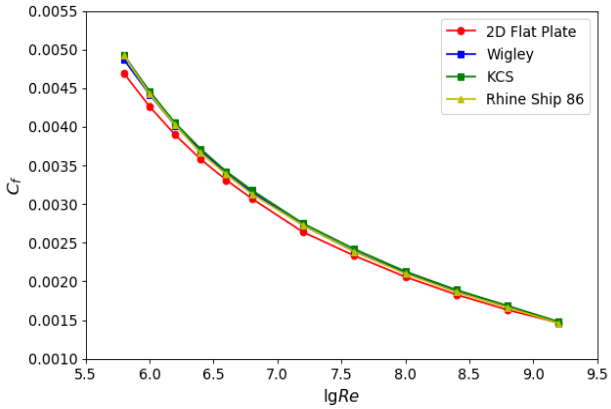

Fig. 9 The results of the frictional resistance coefficient (C_f) against lgRe for the 2D flat plate, the Wigley hull, the KCS, and the Rhine Ship 86 (deep water)

4.1.2 Comparison between the Wigley hull, the KCS, and the Rhine Ship 86

The results of C_f in various water depth for the three ship types are illustrated in **Fig. 10, Fig. 11,** and **Fig. 12**.

From **Fig. 10-12**, although the friction curves of the ships in deep water are similar, they show more significant differences in shallow water. This is caused by the differences in the area of the flat bottom and a different block coefficient (C_B), where the C_B for the Wigley hull, the KCS, and the Rhine ship 86 are 0.45, 0.65 and 0.86. However, the increase of C_f for the KCS and the Rhine ship 86 are similar, but shallow water effects on the Wigley hull are minor. It means that the dependency of C_f on the block coefficient is nonlinear in shallow water.

To find a method for predicting the frictional resistance in shallow water, a two-step regression is made. First, based on the results in deep water, a formula is fitted with MATLAB. The format is similar to the ITTC57 line and shown as follows:

$$C_{f\_deep} = \frac{0.08468}{(\lg Re - 1.631)^2}. \tag{8}$$

Secondly, considering shallow water effects, the correlation line can be given as

$$C_f = \frac{0.08468}{(\lg Re - 1.631)^2} \cdot \left(1 + \frac{c_1}{\lg Re + c_2} \cdot \left(\frac{h}{T}\right)^{c_3}\right), \tag{9}$$

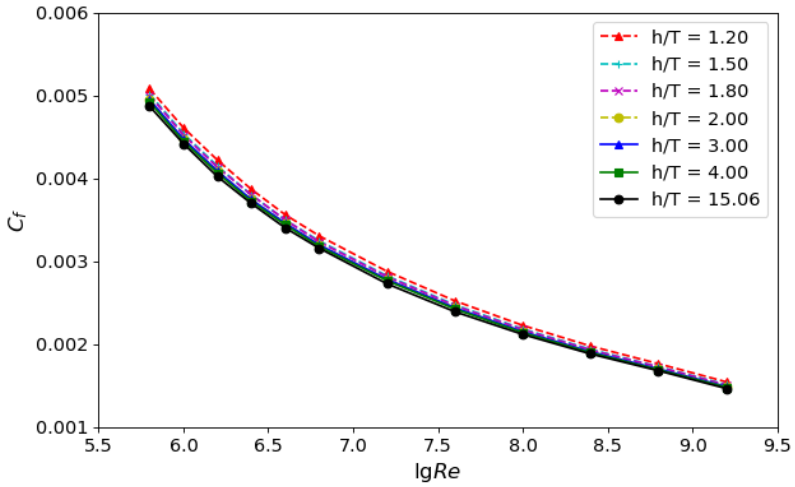

Fig. 10 The frictional resistance coefficient (C_f) against lg*Re* in different water depth for the Wigley hull

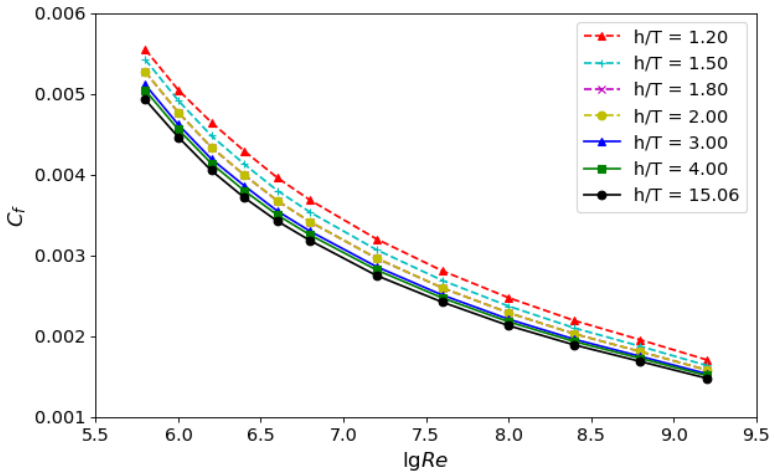

Fig. 11 The frictional resistance coefficient (C_f) against lg*Re* in different water depth for the KCS

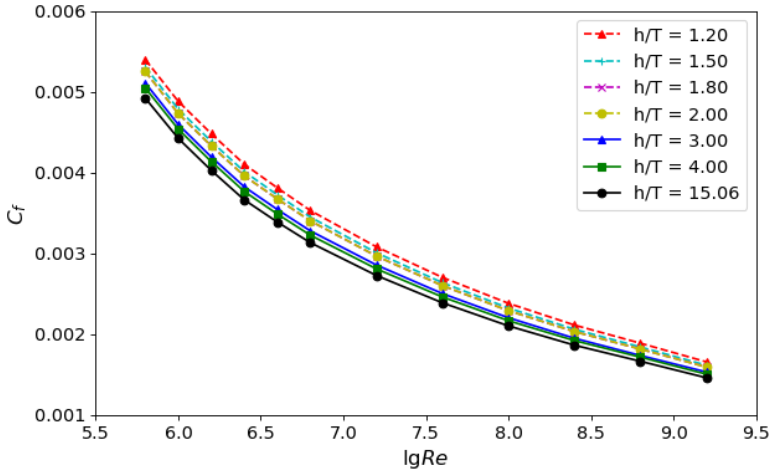

Fig. 12 The frictional resistance coefficient (C_f) against lg*Re* in different water depth for the Rhine Ship 86

Re — Reynolds number;
h — the water depth;
T — the draft of the ship.
The c_1, c_2, and c_3 are constants determined by ship types. The expression (9) is considered to be suitable for the selected three ships sailing at the designed draft in shallow water. The corresponding constants can be fitted with 95% confidence bounds, which are provided in **Table 7**.

Table 7 The c_1, c_2 and c_3 for the Wigley hull and the Rhine Ship 86

	c_1	c_2	c_3
Wigley hull	0.3466	-0.4909	-1.461
KCS	1.2050	-0.5406	-1.451
Rhine Ship 86	1.1680	-0.5238	-1.472

Due to the nonlinear dependency on the block coefficient, more ship forms are required to provide enough data to include ship's parameters into the correlation line.

4.2 The viscous pressure resistance

Due to the influence of viscosity, the water is losing kinetic energy when it passes from the bow to the stern and forms a pressure difference. The resistance caused by this kinetic energy loss is called the viscous pressure resistance. In this subsection, a new definition of the form factor is proposed based on the physical phenomenon in shallow water. The computational results of the three chosen ships are analyzed in sequence with this newly-defined form factor.

4.2.1 A new definition of form factor in shallow water

In shallow water, as shown in Section 4.1, the ship's friction is affected by limited water depth. If a flat plate friction line is still used in the definition of form factor, the form factor will contain shallow water effects on the friction and the viscous pressure resistance simultaneously, which weakens its physical meaning. To remedy this, the computed friction coefficient (C_{f_c}) of the ship is suggested to define the form factor in shallow water. To distinguish it from conventional way, an asterisk is used:

$$1+k^* = \frac{C_v}{C_{f\_c}}. \tag{10}$$

By this definition, the factor k^* clearly represent the viscous pressure resistance. Meanwhile, the $1+k^*$ is not expected to be constant with ship scales, since its Reynolds number dependency is observed to be even extended in shallow water.

In principle, it is required to keep the influence of transom outside the form factor (ITTC, 2017) but it is hard to put into practice in shallow water ship research. For a large number of inland ships, the immersed transom is common, as well as the backward facing tunnel endings. Their effects are already included in the form factor derived from e.g. double-body computations. There are, at least to the authors' knowledge, no reliable method to separate it precisely from form factor.

Physically, the influence of the transom is also a part of viscous pressure resistance thus for practical reasons we consider it as form effects. Therefore, keeping such influence inside the form factor is also nominally acceptable. Based on this, the $1+k^*$ can be seen as an indicator to show transom effects on the viscous pressure resistance of a quite number of inland vessels.

4.2.2 Form factor of the Wigley hull

As shown in **Fig. 13**, the CFD results of $1+k^*$ against the lgRe for the Wigley hull are demonstrated.

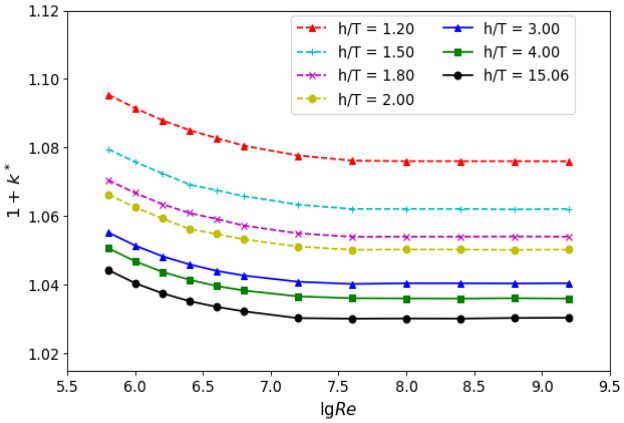

Fig. 13 The form factor against lgRe for the Wigley hull with different water depths

Based on **Fig. 13**:

- The $1+k^*$ decreases with Re when lgRe < 7.2 and becomes stable for higher Re;
- A smaller h/T indicates a higher $1+k^*$ and the curves of $1+k^*$ for different water depth are approximately parallel;
- Water depth affects the $1+k^*$ more than the Re. For h/T = 1.2, the$1+k^*$ increases by about 5%, which is no longer negligible.
- For the same h/T, smaller $1+k^*$ is usually observed for a relatively higher Re. It can be explained by a thinner boundary layer at a higher Reynolds number, where a smaller proportion of kinetic energy is dissipated.

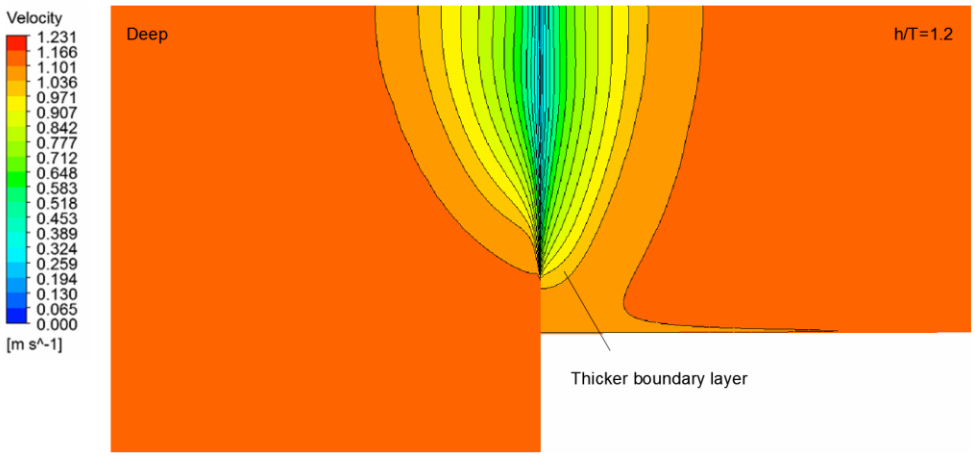

Fig. 14 The velocity distribution at the stern section (x=0m) for h/T=15.06 (part) and h/T=1.20 when lg(Re)=6.4 for the Wigley hull

The presence of water bottom provides an additional boundary layer and will interact with the ship's boundary layer when the water is shallow enough. **Fig. 14** shows a comparison of the velocity distribution at the stern section when lgRe = 6.4. As indicated in the figure, the ship's boundary layer enlarges in the shallow water case particularly in the region where the interaction of the two boundary layers occurs. The water at the stern, therefore, will be less likely to go back to its previous velocity after passing by the ship hull.

A regression of the form factor depending on both the Reynolds number and water depth is proposed for the Wigley hull:

$$(1+k^*)_{Wigley} = \left(1.03 + \frac{1.276}{(\lg Re - 3.277)^{4.79}}\right) \cdot \left(1 + 0.06303 \cdot \left(\frac{h}{T}\right)^{-1.7}\right). \quad (11)$$

The first part of (11) represents the form factor in deep water, and the second part represents the shallow water effects. This formula is valid for $h/T \geq 1.2$, which is in line with the minimum water depth in the calculations.

4.2.3 Form factor of the KCS

Numerical results of $1+k^*$ for the KCS are depicted in **Fig.15**. Similar to the Wigley hull, the form factor becomes stable for lgRe > 7.2. However, the response of the KCS is more significant than the Wigley hull. For h/T = 1.2, the maximum change of $1+k^*$ caused by Re is about 8.6%. Additionally, for the same Re, shallow water effects can cause about 18 % increase of $1+k^*$ at h/T = 1.2 and lgRe = 5.8.

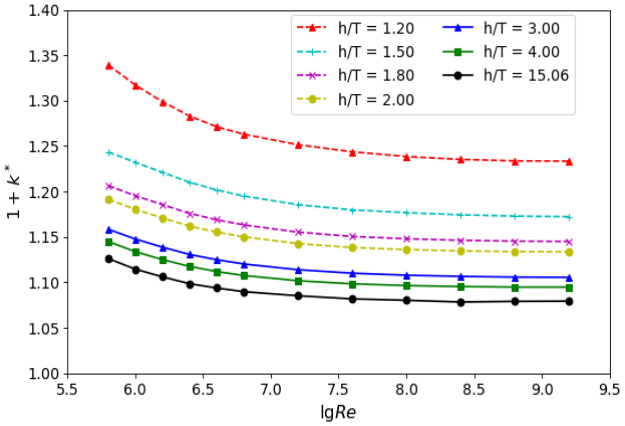

Fig. 15 The form factor against lgRe for the KCS with different water depths

Based on the numerical results, similar to the Wigley hull, the prediction of $1+k^*$ for the KCS can be fitted as

$$(1+k^*)_{KCS} = \left(1.075 + \frac{1.086}{(\lg Re - 3.419)^{3.513}}\right) \cdot \left(1 + 0.2066 \cdot \left(\frac{h}{T}\right)^{-1.887}\right) \quad (12)$$

4.2.4 Form factor of the Rhine Ship 86

For a thin and streamlined surface like Wigley hull, flow separation and vorticity are not observed. However, for ships with a transom like the Rhine Ship 86, vortices are generated behind the stern and the conclusions about the form factor derived from the previous sections may be subject to change.

The results of $1+k^*$ against the lgRe for the Rhine Ship 86 in different water depths are displayed in **Fig. 16**. The $1+k^*$ of the Wigley hull at h/T = 15.06 and h/T = 1.20 are also displayed for comparison.

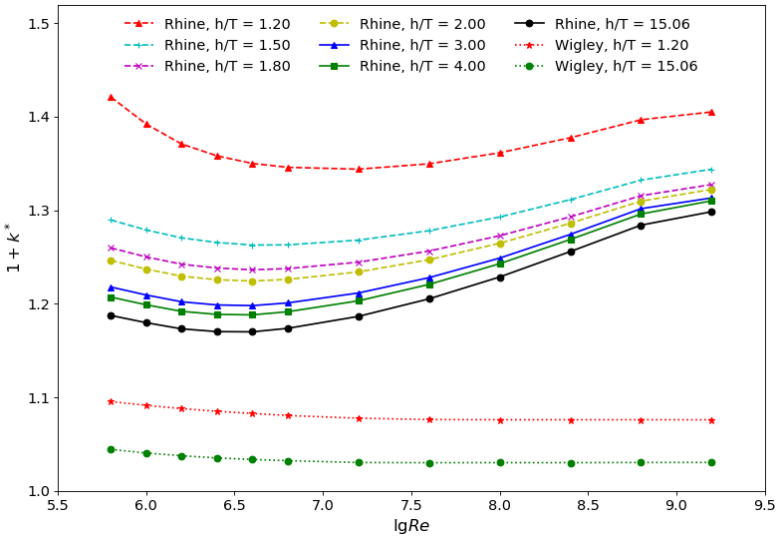

Fig. 16 The form factor against lg*Re* for the Rhine Ship 86 in deep and shallow water

From **Fig. 16** it can be seen that:

- Compared with the Wigley hull, designs with an immersed transom such as the Rhine Ship 86 show a more obvious dependency on Reynolds number;
- The form factor highly depends on the water depth, regardless of whether the Wigley hull or the Rhine Ship 86 is considered, and a higher form factor is observed at a lower *h/T* ratio for both hull forms;
- The form factor is increasing faster with a decreasing *h/T* ratio for the Rhine Ship 86 when compared with the Wigley hull.

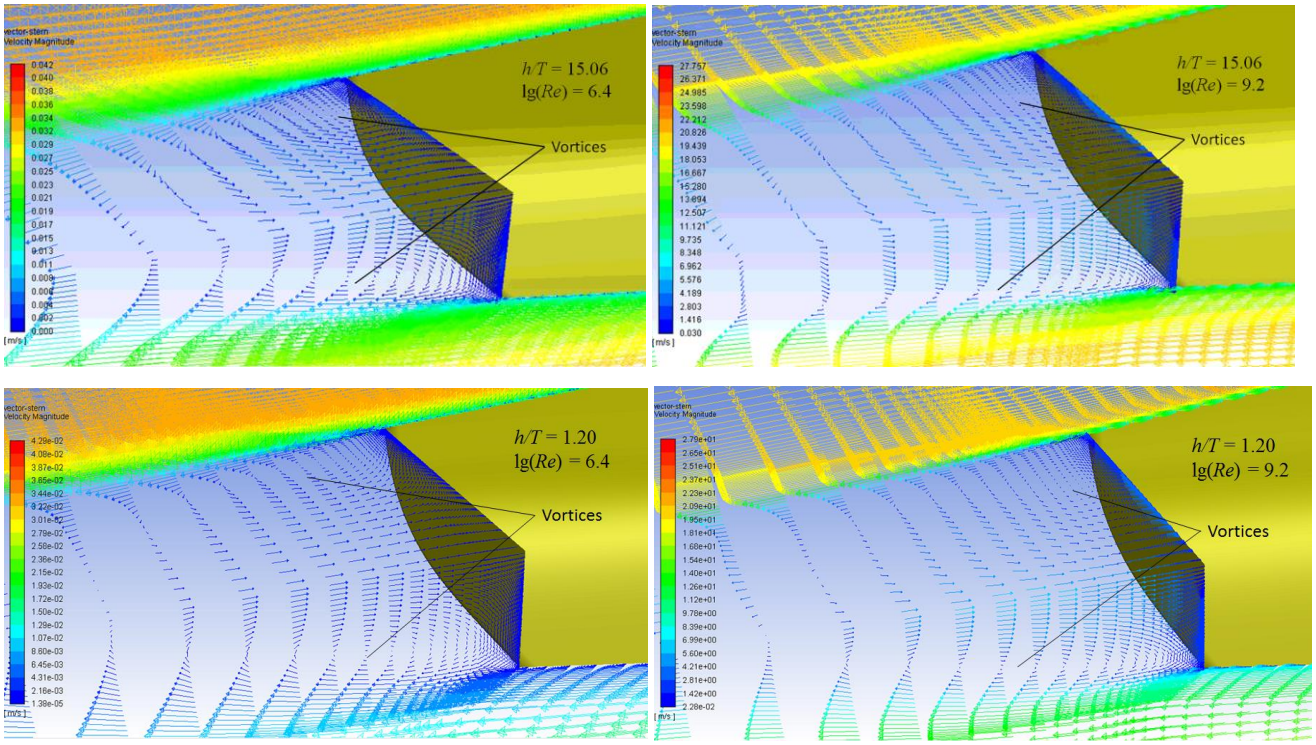

Fig. 17 The vortices generated after the stern for lg*Re* = 6.4 and lg*Re* = 9.2 in deep water (top) and shallow water (bottom)

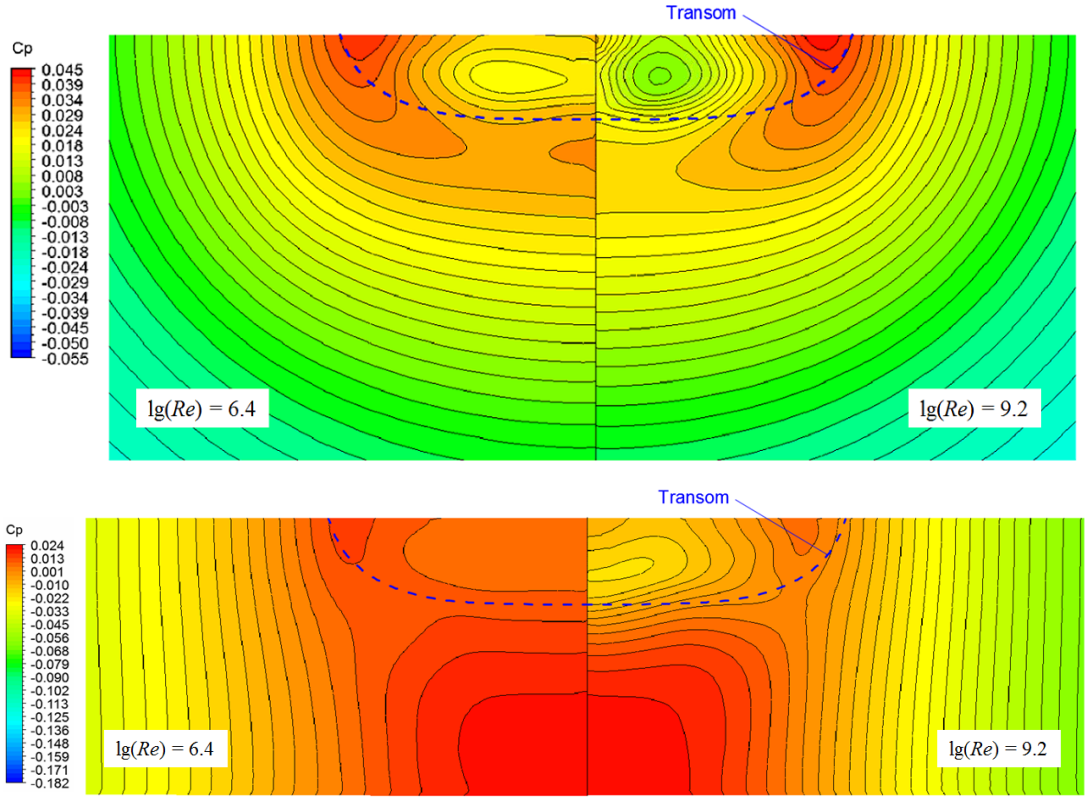

Fig. 18 The contours of pressure coefficient (pressure/($0.5\rho V^2$)) at the section x=-2.5%L after the stern for lgRe = 6.4 and lgRe = 9.2 at deep water (top) and h/T = 1.2 (bottom)

In contrast to the Wigley hull, the $1+k^*$ of the Rhine Ship 86 begin to increase when lg$Re \geq 7.0$. This can be explained by the vortices formed due to the blunt stern and/or the transom. A vertical vortex and a horizontal vertex, as shown in **Fig. 17**, are generated and their cores are interconnected which provides a low-pressure region behind the stern. For a relatively high Reynolds number, the pressure in the vortex core is even lower, both for deep water and shallow water (**Fig. 18**). This can lead to a larger pressure difference between the bow and the stern, which determines a larger $1+k^*$.

Compared with the influence of the 3D boundary layer, which leads to a smaller $1+k^*$ at higher Re, the vortex plays the opposite role and is dominant for lg$Re \geq 7.0$. **Fig. 19** shows a qualitative demonstration of the contributions of ①ship's boundary layer and ②ship's form effects (e.g. vortex) to the $1+k^*$ against the Reynolds number.

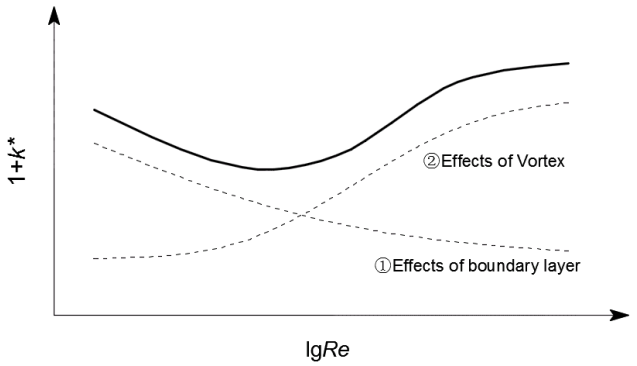

Fig. 19 A qualitative demonstration of the contributions of the 3D boundary layer and the vortex to the $1+k^*$ against the Reynolds number for the Rhine Ship 86

Ship's form, water depth, and the transom can all be counted as form effects, therefore the "form factor" is still nominally appropriate to describe the viscous pressure resistance for a ship with a transom. An adjusted formula considering shallow water effects and the transom is suggested for Rhine Ship 86 for $h/T \geq 1.2$:

$$(1+k^*)_{RhineShip86} = (1+k^*)_{Wigley} + \left(-0.004165 \cdot (\lg Re)^3 + 0.1085 \cdot (\lg Re)^2 - 0.8726 \cdot \lg Re + 2.367\right) \cdot \left(1+1.269\times10^4 \cdot (\lg Re)^{-6.155} \cdot (h/T)^{-4.04}\right) \quad (13)$$

The first part of (13) is the form factor of the Wigley hull, which shows the basic effects of the boundary layer caused by a mildly curved ship, corresponding to curve ① in **Fig. 17**. The remaining part of (13) represents the effects of ship form, such as an altered boundary layer, ship-generated vortices, etc., corresponding to curve ② in **Fig. 17**. It should notice that the remaining part of (13) can be improved by including more physical parameters, such as the geometric parameters of the transom, but a study of various hull forms are subject to further investigations.

4.3 The significance of shallow water effects

In the previous sections, shallow water effects on the viscous resistance of three ships are studied and empirical expressions are fitted. It will be valuable and also straightforward to show the significance of how the viscous resistance deviates from that in deep water.

According to ITTC guidelines (ITTC, 2011), the total resistance of a full-scale ship can be extrapolated from a model test through

$$C_{ts} = (1+k_s)C_{fs} - (1+k_m)C_{fm} + C_{tm} \quad (14)$$

The C_t is the total resistance coefficient, and the subscript s and m represent full scale and model scale, respectively. In the guidelines, the C_f is calculated by the ITTC57 correlation line and the $1+k$ is obtained by the method of Prohaska. However, based on this study, shallow water effects can lead to larger discrepancies for the frictional resistance. In this paper, another definition of the form factor $1+k^*$ is proposed to ensure the C_f include shallow water effects by which its physical meaning is strengthened. An example is given in **Table 8** where the increase of C_f, $1+k^*$, and $(1+k^*)$ C_f caused by shallow water effects are shown for the three ships at h/T = 1.2. Based on **Table 8**, it is found that:

- Both the C_f and $1+k^*$ can have more than 10% increases in shallow water. The increase of $(1+k^*)C_f$ can even reach 30% for the KCS and the Rhine Ship 86;
- Not only the form factor depends on the ship's form, the C_f is also affected and the discrepancy can be as large as 15%.

Therefore, the extrapolation method given by equation (14) should be reevaluated in shallow water. Following the format of equation (14), a similar method is suggested as follows:

$$C_{ts} = (1+k_s^*)C_{fs} - (1+k_m^*)C_{fm} + C_{tm}, \quad (15)$$

Table 8 The increase of C_f, $1+k^*$, and $(1+k^*)$ C_f caused by shallow water effects for three ships (h/T = 1.2)

lg(*Re*)	Wigley hull			KCS			Rhine Ship 86		
	C_f	$1+k^*$	$(1+k^*)$ C_f	C_f	$1+k^*$	$(1+k^*)$ C_f	C_f	$1+k^*$	$(1+k^*)$ C_f
5.8	4.37%	4.89%	9.47%	12.61%	18.92%	33.92%	10.22%	19.66%	31.89%
6.0	4.37%	4.90%	9.48%	13.06%	18.17%	33.61%	12.88%	18.00%	33.20%
6.2	4.97%	4.86%	10.07%	14.73%	17.42%	34.72%	15.13%	16.85%	34.52%
6.4	4.64%	4.81%	9.68%	15.53%	16.79%	34.94%	16.65%	16.06%	35.38%
6.6	4.68%	4.76%	9.66%	15.68%	16.22%	34.45%	17.53%	15.39%	35.62%
6.8	4.73%	4.68%	9.63%	15.81%	15.89%	34.22%	17.99%	14.67%	35.29%
7.2	5.50%	4.60%	10.35%	16.42%	15.31%	34.24%	18.52%	13.27%	34.24%
7.6	5.49%	4.47%	10.21%	16.21%	14.96%	33.59%	18.84%	11.98%	33.08%
8.0	5.15%	4.45%	9.83%	16.29%	14.64%	33.31%	19.01%	10.81%	31.88%
8.4	5.05%	4.45%	9.73%	16.07%	14.54%	32.94%	19.16%	9.69%	30.71%
8.8	5.03%	4.44%	9.69%	15.88%	14.32%	32.47%	19.23%	8.77%	29.70%
9.2	5.45%	4.42%	10.12%	15.43%	14.27%	31.90%	19.29%	8.21%	29.09%

where the C_f should be given by a prediction method of ship's frictional resistance considering shallow water effects, as the examples shown in Section 4.1.2. The $1+k^*$ should be calculated with the method proposed in Section 4.2, where for vessels similar to the three selected ships, the empirical formulas can be applied directly. For other ships, a more general prediction of the form factor needs to be further established. However, the method proposed in this study provides a physically-correct approach to create a formula that is generally applicable to various ships in a range of water depth, and this formula will be the target of the research in the next stage.

5 Conclusions

In this study, the viscous resistance of a ship sailing in shallow water is investigated. Comparisons between a 2D flat plate and three ship forms are made to illustrate the effects of a curved surface on the viscous resistance in deep water. Comparisons of a specific ship in varied vertical-restricted waters are made to show the influence of water depth. Comparisons among the Wigley hull, the KCS, and the Rhine Ship 86 are made to demonstrate how ship forms play a role on the viscous resistance in shallow water. Finally, empirical expressions are fitted for the frictional resistance and the newly-defined form factor.

Based on the results and analyses, several conclusions can be drawn for the ship's viscous resistance in shallow water:

- In contradiction with traditional assumptions based on ships sailing in deep water, the frictional resistance depends on both hull form and water depth in shallow water. A formula to predict ship's friction in shallow water can be built with some constants to be determined based on ship forms;
- The viscous pressure resistance is also affected by hull form and water depth. A definition of the form factor based on the computed frictional resistance instead of the flat plate friction line is proposed to ensure a stronger physical basis. Empirical expressions for the newly-defined form factor of three ships are built considering the effects of both ship scale and water depth;
- For the extrapolation of ship's viscous resistance from model scale to full scale in shallow water, the traditional method excluding shallow water effects will lead to 10% ~ 30% errors in the prediction of the viscous resistance. A method based on the modified friction line and the newly-defined form factor is suggested which provides an idea to make a physically-correct extrapolation for ship resistance in shallow water.

Acknowledgment

This research is funded by the China Scholarship Council (CSC), No.201506950009. The authors also appreciate the Cartesius (the Dutch national supercomputer) with the pilot project No.17172, based on which all computations in this study are realized.

References

ANSYS, 2017. ANSYS® Academic Research, Release 18.1, Help System, Fluent User's Guide. Ansys Inc.

Eça, L., Hoekstra, M., 2009. Evaluation of numerical error estimation based on grid refinement studies with the method of the manufactured solutions. Computers & Fluids 38 (8), 1580-1591.

Eça, L., Hoekstra, M., 2014. A procedure for the estimation of the numerical uncertainty of CFD calculations based on grid refinement studies. Journal of Computational Physics 262, 104-130.

García-Gómez, A., 2000. On the form factor scale effect. Ocean Engineering 27 (1), 97-109.

Grigson, C., 1999. A planar friction algorithm and its use in analysing hull resistance. Trans. RINA 142, 76-115.

Hollenbach, U., 2009. Pro's and Con's of the form-factor using Prohaska's method when extrapolating the model resistance, STG Annual Meeting, Hamburg, pp. 18–20.

Holtrop, J., Mennen, G., 1982. An approximate power prediction method. International shipbuilding progress 29, 166-170.

ITTC, 1957. 8th International Towing Tank Conference, Madrid, Spain.

ITTC, 2008. Specialist Committee on Powering Performance Prediction - Final Report and Recommendations, 25th International Towing Tank Conference.

ITTC, 2011. The Resistance Committee: Final Report and Recommendations, 26th International Towing Tank Conference, pp. 1-50.

ITTC, 2017. Resistance test-Recommended procedures and guidelines 7.5-02-02-01, Proceedings of the 28th International Towing Tank Conference, Wuxi, China.

Jiang, T., 2001. A new method for resistance and propulsion prediction of ship performance in shallow water, Proceedings of the 8th International Symposium on Practical Design of Ships and Other Floating Structures, Shanghai, China.

Kajitani, H., Miyata, H., Ikehata, M., Tanaka, H., Adachi, H., Namimatsu, M., Ogiwara, S., 1983. The summary of the cooperative experiment on Wigley parabolic model in Japan. TOKYO UNIV (JAPAN).

Katsui, T., Asai, H., Himeno, Y., Tahara, Y., 2005. The proposal of a new friction line, Fifth Osaka colloquium on advanced CFD applications to ship flow and hull form design, Osaka, Japan.

Kozioł, A., 2013. Three-dimensional turbulence intensity in a compound channel. Journal of Hydraulic Engineering 139 (8), 852-864.

Lackenby, H., 1963. The effect of shallow water on ship speed. Shipbuilder and Marine Engineer 70, 446-450.

Lee, Y.-G., Ha, Y.-J., Lee, S.-H., Kim, S.H., 2018. A study on the estimation method of the form factor for a full-scale ship. Brodogradnja: Teorija i praksa brodogradnje i pomorske tehnike 69 (1), 71-87.

Millward, A., 1989. The effect of water depth on hull form factor. International shipbuilding progress 36 (407), 283-302.

Pope, S.B., 2000. Turbulent Flows. Cambridge University Press. p.271-275.

Prohaska, C., 1966. A simple method for the evaluation of the form factor and low speed wave resistance. Proceedings 11th ITTC.

Raven, H., 2012. A computational study of shallow-water effects on ship viscous resistance, 29th symposium on naval hydrodynamics, Gothenburg.

Raven, H., 2016. A new correction procedure for shallow-water effects in ship speed trials, Practical Design of Ships and Other Floating Structures 2016, Copenhagen, Denmark.

Roache, P.J., 1998. Verification and validation in computational science and engineering. Hermosa, Albuquerque, New Mexico.

Schlichting, O., 1934. Ship resistance in water of limited depth-resistance of sea-going vessels in shallow water (translated by Roemer, M.C, 1940). Jahrbuch Der STG 35, 127-148.

Toxopeus, S.L., 2011. Viscous-flow calculations for KVLCC2 in deep and shallow water, MARINE 2011, IV International Conference on Computational Methods in Marine Engineering, Lisbon, Portugal.

Van der Ploeg, A., Raven, H., Windt, J., Leroyer, A., Queutey, P., Deng, G., Visonneau, M., 2008. Computations of free-surface viscous flows at model and full scale—a comparison of two different approaches, Proceedings of the 27th symposium on naval hydrodynamics, Seoul.

Zeng, Q., Thill, C., Hekkenberg, R., 2018. A benchmark test of ship resistance in extremely shallow water, Progress in Maritime Technology and Engineering: Proceedings of the 4th International Conference on Maritime Technology and Engineering (MARTECH 2018), Lisbon, Portugal. CRC Press, p. 221.

Zeng, Q., Thill, C., Hekkenberg, R., Rotteveel, E., 2019. A modification of the ITTC57 correlation line for shallow water. Journal of marine science and technology 24 (2), 642-657.